DNA-uptake pilus of *Vibrio cholerae* capable of kin-discriminated auto-aggregation

David. W. Adams, Sandrine Stutzmann, Candice Stoudmann and Melanie Blokesch*

Laboratory of Molecular Microbiology, Global Health Institute, School of Life Sciences, Station 19, EPFL-SV-UPBLO, Swiss Federal Institute of Technology Lausanne (Ecole Polytechnique Fédérale de Lausanne; EPFL), CH-1015 Lausanne, Switzerland.

*For correspondence email: melanie.blokesch@epfl.ch.

Abstract

Natural competence for transformation is a widely used and key mode of horizontal gene transfer that can foster rapid bacterial evolution. Competent bacteria take-up DNA from their environment using Type IV pili, a widespread and multi-purpose class of cell surface polymers. However, how pili facilitate DNA-uptake has remained unclear. Here, using direct labelling, we show that in the Gram-negative pathogen *Vibrio cholerae* DNA-uptake pili are highly dynamic and that they retract prior to DNA-uptake. Unexpectedly, these pili can self-interact to mediate auto-aggregation of cells into macroscopic structures. This phenotype is conserved in disease causing pandemic strains. However, extensive strain-to-strain variability in the major pilin subunit PilA, present in environmental isolates, controls the ability of pili to interact without affecting transformation. We go on to show that interactions between pili are highly specific, enabling cells producing pili composed of different PilA subunits to discriminate between one another. On chitin surfaces, a natural habitat of *V. cholerae*, pili connect cells within dense networks, suggesting a model whereby DNA-uptake pili function to promote inter-bacterial interactions during surface colonisation. Moreover, our results provide evidence that type IV pili could provide a simple and potentially widespread mechanism for bacterial kin recognition.

Keywords

Auto-aggregation, DNA uptake, natural transformation, pilus dynamics, type IV pilus, *Vibrio cholerae*

Introduction

How bacteria physically sense and interact with their environment is a fundamental problem in biology. Type IV pili (T4P) are cell surface polymers ideally suited to this task[1,2]. Composed of a single major pilin and assembled by widely distributed and conserved machinery, T4P exhibit extensive functional versatility, with roles in motility, DNA-uptake, surface sensing and adhesion[3-5]. Consequently, T4P are critical virulence factors for a number of important human pathogens including *Vibrio cholerae*, which causes the pandemic diarrhoeal disease cholera[6]. In Gram-negative bacteria pilins are processed at the inner-membrane, extracted by the assembly machinery and polymerised into a helical pilus fibre that exits the cell surface through a gated outer-membrane pore; the secretin[7-11]. A key feature of T4P is their ability to undergo dynamic cycles of extension and retraction[12,13], powered by the action of dedicated extension (*e.g.* PilB) and retraction (*e.g.* PilT) ATPases, which either add or liberate pilin subunits at the base[14,15]. These dynamics are essential for many T4P functions *e.g.* twitching-motility[11,12]. Thus, understanding how T4P function may yield insights valuable for understanding mechanisms of environmental survival and pathogenesis.

Despite their multifunctional potential, pandemic strains of *V. cholerae* typically encode three distinct T4P systems – two of which are well characterised. First, toxin co-regulated pili (TCP) serve a dual role as both a receptor for CTXϕ bacteriophage[16], which carries the cholera toxin genes, and as the primary human colonisation factor with multiple essential roles in infection involving adhesion and auto-aggregation on the intestinal cell surface[17-19]. Second, Mannose-sensitive haemagglutinin (MSHA) pili are involved in surface sensing and attachment and thus, are important in the initiation of biofilm formation[20-24]. Third, in its natural aquatic environment *V. cholerae* often associates with chitinous surfaces[25], which are nutritious, foster biofilm formation and likely play a role in environmental dissemination and transmission to humans[26-29]. Chitin utilisation triggers competence for natural transformation[30], a widely used mode of horizontal gene transfer

that allows bacteria to take up DNA from their environment, and which can thus, foster rapid bacterial evolution[31]. This requires the production of the Chitin-Regulated (ChiRP) or DNA-uptake pilus[30].

We previously showed DNA-uptake pili form *bona fide* pili composed of the major subunit PilA and that transformation was dependent on the presumed retraction ATPase PilT[32]. However, the pilus itself is not sufficient for transformation and requires the concerted action of a periplasmic DNA-binding protein, ComEA[32,33]. Upon receipt of transforming DNA ComEA switches from a diffuse to focal localisation[33,34]. These findings, together with work in other organisms, led to a model in which pilus retraction facilitates DNA entry into the periplasm[35], wherein ComEA acts as 'ratchet' to pull in the remaining DNA[33]. Subsequently, DNA transport across the inner-membrane occurs via a spatially coupled channel, ComEC[34,36]. Though this model is well supported by genetic experiments[32] and the similarly combined action of T4P and ComEA in other organisms[37,38], direct evidence is lacking.

Here, we visualised the DNA-uptake pilus directly using a cysteine labelling approach, which was recently validated as a tool for labelling pili[39]. As predicted, we demonstrate that the pili are highly dynamic and that these dynamics are PilT-dependent. Unexpectedly, however, we discovered that DNA-uptake pili are also capable of self-interacting, which in liquid culture results in a strong auto-aggregation phenotype. Variability in PilA controls this activity but has no affect on transformation. Remarkably, specific interactions allow pili composed of different PilA subunits to distinguish between one another, enabling a simple mechanism for kin recognition.

Results

Direct observation of pilus dynamics by cysteine labelling

To avoid the limitations imposed by immuno-fluorescent methods, we employed a cysteine labelling approach using a thiol-reactive dye[39,40]. PilA cysteine variants were created along the length of the surface exposed αβ-loop[9,11] and tested for functionality using a previously validated chitin-independent transformation system in which competence induction is arabinose-inducible[41] (Tn*tfoX*; see methods) (Fig. 1A, B and Fig. S1A). A variant, PilA[S67C], was identified that relative to the unmodified parent is fully transformable (Fig.1A), produced at similar levels (Fig. S1B), and does not affect pilus assembly (Fig. S1C), as assayed by a classical shearing method. Since other variants exhibited functional defects they were not studied further.

When stained, competent cells producing PilA[S67C] exhibited visible pili (Fig. 1C). On average 27 ± 3 % cells were piliated, with the majority of these displaying 1 or 2 pili per cell (Fig. 1H and I). The length of pili was clustered around 1-2 µm, though pili up to 10 µm in length were also observed (Fig. 1J). Numerous detached pili were also evident in the growth media. Intriguingly, these pili frequently appeared to self-interact, forming large structures composed of networks of pili (Fig. S2A). When examined by time-lapse microscopy cells exhibited rapid pilus dynamics, with multiple assembly and retraction events immediately apparent (Fig. 1K; Movie S1-4). Indeed, within the 1 minute time frame studied 66 ± 3 % cells exhibited pili, with most cells producing 1-2 pili per minute (Fig. 1M). Notably, a small subpopulation of cells was even more dynamic, elaborating ≥5 pili per minute. Consistent with this dynamic behaviour, and in support of the hypothesis that pilus retraction precedes DNA-uptake, when cells were provided with purified genomic DNA it was possible to concurrently visualise pilus retraction followed by DNA-uptake, as monitored by the re-localisation of ComEA-mCherry, which binds incoming DNA in the periplasm (Fig. S3; Movie S5).

As expected, deletion of components required for pilus assembly (*e.g.* the assembly ATPase PilB or the secretin PilQ) abolished piliation (Fig. 1D and E). However, despite the absence of obvious pili the cell body still stained. Control experiments in which PilA[S67C], but not PilA[WT], was produced independently of the normal assembly machinery also stained similarly (Fig. S1D), suggesting that this effect results from the dye being taken up non-specifically and retained by the inner-membrane pool of PilA[S67C].

As in other species *V. cholerae* encodes two potential retraction ATPases, PilT and PilU. Deletion of *pilU* did not affect piliation (Fig. 1F, H and I), consistent with its dispensability for transformation[32]. In contrast, cells lacking the presumed retraction ATPase PilT were hyper-piliated, with essentially all cells displaying multiple static pili (Fig. G-I; Movie S6-7). Taken together with the dynamics described above, these data are consistent with the presence of multiple assembly complexes scattered across the cell, as previously predicted based on the mobility of PilB and the presence of multiple PilQ foci[32,42]. This might normally serve to facilitate rapid switching of pilus location or else might reflect a need to produce multiple pili under certain conditions. Unexpectedly, cells blocked for retraction were often grouped into small clusters within dense networks of pili as well as occasionally large aggregates of pili-encased cells (Fig. S2B and C). Indeed, when grown in liquid culture cells appeared to auto-aggregate.

Competent cells auto-aggregate in the absence of pilus retraction

To test directly whether the aggregation phenotype was an inherent property of hyper-piliated cells or merely an artefact introduced by the cysteine variant, cells containing unmodified *pilA* were examined (Fig. 2A-C). Remarkably, aggregation occurred specifically in competence-induced cells lacking *pilT*, with the formation of large, multi-layered spherical aggregates on the order of 25-100 µm, which went on to form macroscopic aggregates that rapidly sediment (Fig. 2B, +Ara). Quantification of the ratio of cells remaining in solution to

133 those in the settled aggregates (Fig. 2D) revealed that upon competence induction, ≥90% of
134 the retraction deficient cells were present in aggregates (Fig. 2D). Notably, strains producing
135 the PilA[S67C] variant used for labelling behave similarly (Fig. 1B).

136 To rule out the possibility that the deletion of *pilT* has either a polar or otherwise
137 non-specific effect, an intact copy of *pilT* driven by its native promoter was placed at an
138 ectopic locus. Importantly, complementation of Δ*pilT* was sufficient to fully restore the
139 ~1000-fold defect in transformation frequency and abolished the aggregation phenotype
140 (Fig. 2D and E). Complementation also fully counteracted the enhanced motility phenotype
141 of Δ*pilT* (Fig. S4), which occurs due to loss of function in the adhesive MSHA pilus and is in
142 agreement with the previously established shared role of PilT in MSHA pilus function[24,43].

143 Time-course experiments indicated that aggregation occurs abruptly, suggesting
144 that rather than gradually increasing in size, large aggregates form via the accumulation of
145 smaller ones (Fig. S5A and B). In support of this hypothesis, when two otherwise isogenic
146 Tn*tfoX* Δ*pilT* strains, one of which constitutively produces GFP, were allowed to aggregate
147 together they formed well-mixed aggregates (Fig. S5E). If, however, they were allowed to
148 aggregate separately before being mixed (Fig. S5C and D), they formed large composite
149 aggregates consisting of a patchwork of labelled and unlabelled cells (Fig. S5F). Finally, the
150 aggregates remained stable and did not disperse, even after prolonged culture overnight.
151

152 **Aggregates form via pilus-pilus interactions**

153 The data so far suggest that hyper-piliated cells auto-aggregate via their DNA-uptake
154 pili. Indeed, deletions affecting DNA-uptake pilus assembly (*pilQ* and *pilA*) were sufficient to
155 abolish aggregation (Fig. 2F). In contrast, deletions targeting the assembly of TCP (*tcpA*) and
156 MSHA (*mshA*) pili, the *Vibrio* polysaccharide matrix (*vpsA*) required for biofilm formation[44] or
157 the flagellum (*flaA*), were dispensable for aggregation, both individually and in combination
158 (Fig. 2F). Similarly, additional genes tested with roles in biofilm formation (*bap1*, *rbmA*,

159 *rbmEF*, *vpsT*)[45,46], adhesion (*gbpA*)[47], cell shape (*crvA*)[48] and an O-linked glycosylase (*VC0393*
160 or $pglL_{Vc}$)[49] that could be involved in pilin modification all aggregated at levels
161 indistinguishable from the unmodified parent (Fig. S6A). Finally, deletion of *VC0502*, an
162 'orphan' type IV pilin encoded on the *Vibrio* seventh pandemic island II, had no effect on
163 transformation, aggregation or motility (Fig. S6B-D). Additional control experiments
164 indicated that aggregation occurred similarly during growth under high salt conditions (*i.e.*
165 LB-S 20 g/L NaCl), which are often used to better reflect the natural aquatic environment of
166 *Vibrio sp*. (Fig. S6E). Likewise, the presence of Bovine serum albumin, which was previously
167 reported to disrupt pilus-pilus interactions in *Neisseria gonorrhoeae*[50], also had no effect
168 (Fig. S6E). Curiously, however, we noticed that the strength of the aggregation phenotype is
169 sensitive to the concentration of divalent cations (*e.g.* $CaCl_2$ or $MgCl_2$) (Fig. S6F), though the
170 significance of this result remains unclear.

171 To investigate how the pilus mediates auto-aggregation *i.e* pilus-pilus, pilus-cell or
172 otherwise, we co-cultured cells producing either dynamic pili (Tn*tfoX*), static pili (Tn*tfoX*,
173 Δ*pilT*), or blocked for both retraction and pilus production (Tn*tfoX*, Δ*pilT*, Δ*pilA*) with a
174 Tn*tfoX* Δ*pilT* strain constitutively producing GFP (Fig. 2G-I) and asked whether these cells
175 were recruited into the GFP-labelled aggregates. Strikingly, intermixed aggregates were only
176 observed when both cells were themselves capable of producing non-retractile pili, and
177 hence aggregating (Fig. 2H), indicating that aggregates form via direct pilus-pilus interactions
178 between DNA-uptake pili.

179

180 **MSHA pili do not mediate aggregation**

181 MSHA pili are important for surface sensing and attachment during the switch to the sessile
182 lifestyle that precedes biofilm formation, and pilus retraction is thought to be required for
183 their function[20-24]. Since MSHA pili are constitutively produced, but retraction deficient cells
184 only aggregate upon competence induction, the results above suggest that MSHA pili are

unable to mediate auto-aggregation. To test this hypothesis directly we grew cells engineered to increase the levels of the second messenger c-di-GMP, which has been reported to enhance the assembly of MSHA pili on the cell surface[43]. Control experiments indicated that decreasing c-di-GMP levels cells did not induce aggregation (Fig. S7A and B). In contrast, under elevated c-di-GMP levels, cells formed large clumps that appeared similar to the aggregates described above and had a modest sedimentation phenotype (Fig. S7A and B). However, the assembly of these structures occurred independently of *pilT*, *pilA* and *mshA*, but was abolished by the loss of *vpsA* (Fig. S7C). Thus, we conclude that these structures are not aggregates held together by pili but rather biofilms held together by matrix polysaccharide.

PilA from pandemic strains is sufficient for aggregation in a non-pandemic strain

A1552, the strain used throughout this work, is an O1 El Tor clinical isolate representative of the on-going 7th cholera pandemic. To test whether the ability to aggregate is conserved among other pandemic strains we tested 6 additional O1 El Tor strains. In the absence of *pilT* all aggregated to similar levels as A1552, as might be expected given that pandemic strains are closely related (Fig. 3A). Surprisingly, however, N16961 did not aggregate unless its well-characterised *hapR* frame-shift mutation[51], which renders it quorum-sensing (QS) defective, was first repaired (Fig. 3A). Since transcription of the genes required for pilus assembly are not regulated by QS[41] this finding suggests that there may be an additional layer of post-transcriptional control.

PilA is known to vary considerably between different environmental strains of *V. cholerae*[52], whereas the majority of clinical isolates carry an identical *pilA*. Interesting exceptions are the toxigenic O37-serogroup strains V52 and ATCC25872, which were responsible for limited epidemics of a cholera-like illness in the 1960s[53,54]. These strains are thought to derive from a pandemic O1 classical strain through the exchange of the O-antigen

211 cluster by horizontal gene transfer[55,56]. However, they both encode the same PilA version
212 that is only 50% identical to that typically carried by pandemic strains (Fig. S8). Since V52 is
213 QS deficient, and transformation is QS dependent, we investigated the functionality of this
214 PilA in ATCC25872, which has a functional QS pathway. Indeed, ATCC25872 is transformable
215 at similar levels to that of A1552, and as expected, transformation is PilT-dependent (Fig.
216 3B). However, in contrast to A1552, competence-induced cells lacking *pilT* did not aggregate
217 and were excluded from aggregates formed by A1552 (Fig. 3C-E, H and I).
218 Given that all the other known components required for pilus assembly and
219 transformation are highly conserved in ATCC25872, we tested whether PilA itself was
220 responsible for this phenotype by exchanging the endogenous *pilA* open reading frame for
221 that of A1552 (*pilA*ex). As expected, the ATCC25872 *pilA*ex strain was fully transformable
222 (Fig. 3B). Importantly, however, in the absence of *pilT*, competence-induced cells of this
223 strain were now able to form large aggregates, albeit at lower levels than in A1552 (Fig. 3C, F
224 and G), and intermix within aggregates formed by A1552 (Fig. 3J and K).
225
226 **PilA variability governs auto-aggregation and enables kin-recognition**
227 The results above suggest that the ability to aggregate is dependent on the particular PilA
228 variant carried. Indeed, BLAST analyses of 647 *V. cholerae* genomes deposited in NCBI
229 indicated that PilA exhibits extensive variation, whereas the other proteins encoded within
230 its operon, as well as those from neighbouring genes, are all highly conserved (Fig. S9). Of
231 the 636 intact *pilA* genes identified, the majority (492/636) encode a PilA identical to that of
232 A1552, which is likely due to an over-representation of patient-derived pandemic strains in
233 the database. Next, we extracted the unique PilA coding sequences (56/636) (Fig. S10A) and
234 combined them with those of an in-house collection of various environmental and patient
235 isolates. The resulting phylogenetic tree consists of around 12 distinct groups and was used
236 to sample PilA diversity (Fig. 4A). As expected, the N-terminal ~50 residues, which contain

237 sequences required for membrane trafficking and pre-pilin peptidase recognition, and that
238 goes on to form the long structural alpha helix (α1), are well conserved (Fig. S10A and B). In
239 contrast, apart from a few clusters of key conserved residues, including the C-terminal
240 cysteines that form the characteristic disulphide-bonded loop, the C-terminal domains are
241 highly variable (Fig. S10A and B).

242 To test how PilA variability affects pilus function but avoid the potential problems of
243 working in various strain backgrounds, we inserted new *pilA* alleles at the native *pilA* locus in
244 strain A1552, and used a short (30 bp) duplication of 3' end of the original *pilA* to maintain
245 any regulation of the downstream genes. We validated this *pilA* replacement (*pilA*rep)
246 approach using A1552 PilA (*i.e.* Tn*tfoX*, *pilA*rep[A1552]), which is fully transformable, and in
247 the absence of *pilT* aggregates at levels similar to the unmodified parent (Fig. 4B and C). We
248 then tested 16 different PilA sequences from across the tree (Fig. 4A and Fig. S10B).
249 Interestingly, all were equally capable of supporting transformation (Fig. 4B). In contrast, the
250 ability to aggregate varied depending on the particular PilA. Indeed, in the absence of
251 retraction, 9/16 PilAs supported the aggregation phenotype, though PilA DRC186-4 was
252 intermediate, whereas 7/16 did not detectably aggregate (Fig. 4A and C).

253 Given that aggregation occurs via direct pilus-pilus interactions we hypothesised
254 that the variability between the different aggregation-proficient PilA might allow pili
255 composed of different PilA to distinguish between one another. To test this idea we used
256 the same co-culture approach as before, using strains with and without constitutive GFP
257 production, and examined all possible combinations (Fig. 4D). As expected, cells producing
258 pili composed of an identical PilA always exhibited uniform mixing (Fig. 4D and E).
259 Remarkably, however, in 41/45 possible unique combinations the interactions between
260 different pili were highly specific (Fig. 4D). Indeed, cells of these strains aggregated in a pilin-
261 specific manner, preferentially forming aggregates with cells producing pili composed of the
262 same PilA. This resulted in aggregates that were either almost exclusively fluorescent or

non-fluorescent (Fig. 4F). In 4/45 cases a partial cross-interaction was observed, resulting in an intermediate mixing phenotype, with aggregates composed of smaller but still segregated groups of cells (Fig. 4D and G). Overall these data indicate that pili composed of different PilA are able to discriminate between one another, probably via specific PilA-PilA interactions. Moreover, these data demonstrate that PilA variability not only determines the ability to aggregate, but also provides a mechanism for kin-recognition.

The TCP is also capable of aggregation under conditions mimicking virulence induction[18,57]. Indeed, in strains artificially induced for virulence TCP-mediated aggregates readily formed that appeared similar to those described in this work (Fig. S11A and C). As expected, they did not intermix with aggregates formed by DNA-uptake pili (Fig. S11B-D). Of note, however, is that TCP are largely limited to pandemic lineages with 2 variants of its major pilin TcpA: Classical and El Tor[58-60]. In contrast to the results above and in line with previous work[58], a classical and El Tor strain formed uniformly mixed TCP aggregates (Fig. S11E), indicating that the different TcpA do not discriminate between one another.

The unusual tail of ATCC25872/V52 PilA is an inbuilt inhibitor of aggregation

To rule out the possibility that strains unable to aggregate simply fail to make sufficient numbers of pili, we made labelable *pilA*rep cysteine variants of A1552 PilA (*pilA*rep[A1552; S67C]) and 2 non-aggregating alleles (*i.e. pilA*rep[Sa5Y; S67C] and *pilA*rep[V52; N67C]). All constructs behaved similarly to the equivalent non-cysteine variant, though the *pilA*rep[Sa5Y; S67C] has a modest transformation defect (Fig. S12A and B). Both the PilA[Sa5Y] and PilA[V52] cysteine variants were piliated at similar levels to the A1552 control and in the absence of *pilT* were hyper-piliated, although pili composed of PilA[Sa5Y] were generally very short (Fig. 5A and B). The hyper-piliation was especially clear for the V52 cysteine variant and provides direct evidence that the inability of some alleles to aggregate is likely not due to a failure to produce sufficient numbers of pili but reflects a specific

289 property of the pilin itself. Notably, sheared pili of the *pilA*rep[A1552; S67C] variant
290 assembled into large structures, as above, whereas those of the others did not (Fig. S12C).
291 Strains V52 and ATCC25872 encode an identical PilA with an unusual repetitive C-
292 terminal extension (SGSGSGSGSGSGSGSGSGN), or 'tail'. Among the PilA sequences analysed
293 here, there were 9 examples of this type of tail clustered into 2 well-separated phylogenetic
294 groups (Fig. S8). Moreover, of the *pilA*rep PilAs unable to support aggregation 3/7 contain a
295 tail (Fig. S8B). Thus, to test if the tail affected V52 PilA function we created a truncated
296 variant *i.e. pilA*rep[V52Δtail], which was similarly transformable to the equivalent tailed
297 version (Fig. 5C). Remarkably, however, removal of the tail restored the ability to aggregate
298 in the absence of *pilT*, at levels indistinguishable from that of the PilA[A1552] controls (Fig.
299 5D), and demonstrated a similar ability to 'recognise' itself in co-culture experiments (Fig.
300 5E). These data suggest that the tail inhibits the ability of pili to aggregate, possibly by
301 masking the site of pilus-pilus interaction. Indeed, a strain in which this tail was transplanted
302 onto PilA of A1552 (*i.e. pilA*rep[A1552+tail] remained highly transformable but was unable
303 to aggregate (Fig. 5C and D). However, since efforts to label this PilA variant have so far been
304 unsuccessful we cannot exclude another, non-specific effect.
305
306 **DNA-uptake pili form networks on chitin surfaces**
307 The data so far indicates that interactions between pili can mediate intercellular contacts.
308 However, in liquid culture this relies on blocking pilus retraction. We reasoned that if these
309 interactions are relevant to the normal ecology of *V. cholerae* then we might be able to
310 detect them under more realistic conditions. Therefore, we visualised pili produced by
311 otherwise WT cells upon cultivation on chitinous surfaces (Fig. 6A). Strikingly, under these
312 conditions of natural induction, cells colonising the chitin surface were generally found
313 embedded within dense networks of pili that were often overlaid by larger pili structures
314 (Fig. 6A). In contrast to the chitin-independent liquid culture experiments, cells on the chitin

surface often appeared to possess multiple pili simultaneously (Fig. 6B), though the crowded nature of the cells precluded direct quantification. Furthermore, since the washing steps required for pilus staining tend to remove cells, but not pili, from the surface, the number of cells engaged in these networks is likely underestimated. Control experiments confirmed that labelling on surfaces is specific and that these structures are DNA-uptake pili (Fig. S13A-C). Notably, Δ*pilT* cells are heavily hyper-piliated under these natural induction conditions (Fig. S13D), indicating that the phenotypes observed in liquid culture are not an artefact of artificial competence induction.

Next, using the *pilA*rep cysteine variants described above, we directly compared the pili assembled on chitin surfaces by cells producing the aggregation-proficient PilA[A1552] with those producing the aggregation-deficient PilA[V52]. Consistent with its functionality in the various assays above, cells carrying *pilA*rep[A1552; S67C] were also found within similar pili networks (Fig. 6C and E). In contrast, such networks were never observed for cells carrying *pilA*rep[V52; N67C] (Fig. 6D and F). Instead, the surfaces were coated in what appeared to be mostly individual pili. This difference was particularly clear at later time-points when cells presumably began to exhaust the chitin surface. Cells producing PilA[A1552] covered surfaces with extensive and long-range networks of pili that were maintained within detached pieces of biofilm (Fig. S14A and C). In contrast, for cells producing PilA[V52] the surfaces were coated with individual pili and never large networks (Fig. S14B and D). In summary, these data suggest that the aggregation phenotypes observed in liquid culture experiments report the natural ability of pili to interact on chitin surfaces.

Discussion

Here we demonstrate that DNA-uptake pili are highly dynamic, that these dynamics are PilT-dependent, and that cells lacking *pilT* are minimally transformable, providing direct evidence

for the longstanding model, whereby pilus retraction facilitates DNA-uptake. Indeed, our results on pilus dynamics are in close agreement with those recently reported by Ellison *et al.*, who notably, went on to demonstrate that the pilus binds directly to DNA[61]. The major finding of this work, however, is that DNA-uptake pili are able to interact and distinguish between one another in a specific manner depending on their sequence. In liquid culture when retraction is blocked this manifests as an exaggerated auto-aggregation phenotype. Since only a subpopulation of cells is piliated at any one time, and these pili are dynamic, blocking retraction likely facilitates auto-aggregation by producing a homogenous population of hyper-piliated cells, thereby increasing the chances of interactions between pili. Work in *Neisseria meningitidis*, which auto-aggregates naturally at low levels but is dramatically enhanced by the deletion of *pilT*, supports this idea[62,63]. Importantly, however, under natural induction conditions on chitin surfaces, cells producing pili capable of aggregation elaborate multiple pili and form dense pili networks in an otherwise unmodified background, indicating that the chitin surface likely promotes interactions between pili. The crowded surface environment might inherently foster these interactions. Alternatively, the altered physiology of cells growing on chitin might also impact pilus assembly via effects on the extension/retraction motors.

The TCP of *V. cholerae* is induced during virulence and is essential for colonisation[18,57,64]. Under laboratory conditions TCP production results in auto-aggregation similar to that described here[17,19,58]. Moreover, in an infection model cells on the intestinal cell surface were found encased within networks of TCP, that were suggested to protect cells from host defences[65]. Given the similarities between the two systems, especially our observation of dense pili networks on colonised chitin surfaces, we propose that the DNA-uptake pilus might play an analogous role in the aquatic environment. Indeed, as hypothesised elsewhere[29,66], since pilus production is dependent on an intact chitin-utilisation pathway, colonisation mechanisms using DNA-uptake pili would be inherently

367 selective for (i) nutritious chitinous surfaces and (ii) favour the recruitment and retention of
368 productive cells while excluding non-productive cells unable to make pili. Thus, intercellular
369 interactions between DNA-uptake pili could act at multiple stages of colonisation, but might
370 be particularly advantageous during early stages to bring smaller chitin particles together,
371 and thus provide resistance to protozoan grazers, as well as at later stages to keep cells
372 together during biofilm dispersal. It remains possible, however, that these interactions
373 represent an ancient colonisation mechanism that has since been replaced. Arguing against
374 this idea is the observation that all pandemic strains retain the same interaction-proficient
375 PilA even though other environmental strains have been free to vary their PilA without
376 impacting its ability to mediate transformation. Interestingly, ingestion of colonised chitin
377 particles is thought to facilitate transmission to humans[26] and recovering cholera patients
378 exhibit a strong immune response to PilA[67]. One possibility that should be investigated is
379 that the networks of DNA-uptake pili we observed on chitin surfaces protect cells during this
380 process.

381 In *Neisseria gonorrhoeae*, artificially varying the density or post-translation
382 modification state of pili leads to a form of cell sorting based on differential interaction
383 forces between pili[68]. This effect is likely related to aggregate dispersal during its infective
384 lifestyle but does not permit specific recognition *per se*[69]. In contrast, the discovery here that
385 the natural variability of PilA controls the ability of pili to self-interact, and creates highly
386 specific interactions, provides a direct mechanism for kin recognition. The best-studied
387 examples of kin recognition in microorganisms all involve adhesins and some form of
388 aggregation (*e.g.* Flo1; *Saccharomyces cerevisiae*[70], TgrB1-TgrC1; *Dictyostelium discoideum*[71],
389 and TraA; Myxobacteria[72]). In evolutionary terms, these recognition mechanisms are
390 classified as 'greenbeards' because the cue, recognition of the cue and the resulting
391 cooperative activity are all encoded by the same gene[73,74]. The ability of DNA-uptake pili to
392 recognise and interact with pili composed of the same kind of PilA fits this classification and

393 is therefore a specific form of greenbeard recognition[73,74]. However, this form of recognition
394 implies close identity only at the greenbeard locus and so is better referred to as kind
395 recognition[73,74].

396 An important question going forward will be to understand what drives PilA diversity
397 and how this is related to the type VI secretion system, which acts to kill non-kin
398 bacteria[75,76]. Similarly, the apparent acquisition of an inhibitor of pilus interactions by some
399 PilA (*e.g.* ATCC25872/V52) hints that the ability to interact may not always be beneficial.
400 Therefore, future work should focus on how the pili networks we observed on chitin
401 surfaces contribute to the ecology of *V. cholerae*, especially under environmental conditions.
402 Indeed, we still know relatively little about the natural lifestyle of *V. cholerae* on chitin, in
403 part due to the inherent technical difficulties associated with manipulating these surfaces.
404 Nevertheless, the demonstration that in liquid media, specific interactions between pili
405 composed of different major pilins is sufficient to enable segregation, provides a robust
406 proof-of-concept that T4P have the ability to function as a recognition mechanism. Finally,
407 the fact that (i) T4P are widespread, (ii) auto-aggregation via T4P has been reported in
408 multiple species[77] and (iii) the major pilin subunit often varies[4,52], raises the possibility that
409 specific interactions between T4P might be quite common and therefore represent an
410 important contribution to bacterial kin recognition worthy of continued investigation.
411

412 **Materials and Methods**

413 **Bacterial strains and plasmids**

414 The bacterial strains used in this study are shown in Supplementary Table S1, together with
415 the plasmids used and their construction. A1552, the *V. cholerae* strain used throughout this
416 work[78], is a toxigenic O1 El Tor Inaba strain representative of the on-going 7th cholera
417 pandemic, and was derived from a traveller entering the United States after being infected
418 on a commercial aeroplane that took off in Peru[79].

419

420 **General methods**

421 Bacterial cultures were grown aerobically at 30˚C or 37˚C, as required. Liquid medium used
422 for growing bacterial strains was Lysogeny Broth (LB-Miller; 10 g/L NaCl, Carl Roth,
423 Switzerland) and solid medium was LB agar. Where indicated, LB-S contained 20 g/L NaCl.
424 Ampicillin (Amp; 100 µg/mL), gentamicin (Gent; 50 µg/mL), kanamycin (Kan; 75 µg/mL),
425 streptomycin (Str; 100 µg/mL) and rifampicin (Rif; 100 µg/mL) were used for selection in *E.*
426 *coli* and *V. cholerae*, as required. To induce expression from the P_{BAD} promoter, cultures
427 were grown in media supplemented with 0.2% L-arabinose. Natural transformation of *V.*
428 *cholerae* on chitin flakes was done in 0.5x DASW (Defined artificial seawater), supplemented
429 with vitamins (MEM, Gibco) and 50 mM HEPES, as previously described[30]. Counter-selection
430 of phenylalanyl-tRNA synthetase (*pheS**) insertions (Trans2 method; see below) was done
431 on medium supplemented with 20 mM 4-chloro-phenylalanine (cPhe; Sigma-Aldrich,
432 Switzerland). Thiosulfate citrate bile salts sucrose (TCBS; Sigma-Aldrich, Switzerland) agar
433 was used to counter-select for *E. coli* following bacterial mating. SacB-based counter-
434 selection was done on NaCl-free medium containing 10 % sucrose.

435

436 **Strain construction**

437 DNA manipulations and *E. coli* transformations were carried out using standard methods[80],
438 and all constructs were verified by PCR and Sanger sequencing (Microsynth AG, Switzerland).
439 Genetic engineering of *V. cholerae* was done using a combination of natural transformation
440 and FLP-recombination; Trans-FLP[81,82], *pheS**-based counter-selection; Trans2[83,84], and allelic
441 exchange using bi-parental mating and the counter-selectable plasmid pGP704-Sac28[29]. The
442 mini-Tn7 transposon carrying *araC* and various P_{BAD}-driven genes was integrated into the
443 large chromosome by tri-parental mating, as previously described[85].

444

445 **Chitin-independent competence induction**

446 Chitin oligosaccharides resulting from growth on chitin trigger natural competence induction
447 via the production of a master regulator, TfoX[29,30,86-88]. High cell-density, as sensed by
448 quorum sensing via HapR, results in the production of an intermediate regulator QstR, which
449 acts in concert with TfoX to regulate the transcription of a subset of the competence
450 genes[30,41,89]. Therefore, to induce natural competence in liquid culture we used a well
451 characterised and already validated chitin-independent approach that results in low levels of
452 TfoX production[41]. This approach is based on the integration of a mini-Tn7 transposon into
453 the large chromosome of *V. cholerae* containing an arabinose-inducible copy of *tfoX* (*i.e.*
454 *araC*, P_{BAD}-*tfoX*), which we refer to as Tn*tfoX*. In the presence of inducer, strains carrying
455 Tn*tfoX* turn on the expression of the competence genes according to the known regulatory
456 pathways and upon reaching high cell-density are transformable at levels similar to those
457 seen on chitin[41]. In the absence of inducer, competence genes are not produced and strains
458 are non-transformable[41].

459

460 **Transformation frequency assay**

461 Diverse strains harbouring Tn*tfoX* were tested for transformation using a chitin-independent
462 transformation frequency assay, as previously described[32,41]. Briefly, overnight cultures were
463 back-diluted 1:100 in fresh media with and without arabinose, as indicated, and grown 3h at
464 30˚C with shaking (180 rpm). 0.5 mL aliquots of the cultures were mixed with 1 µg genomic
465 DNA (GC#135; A1552-lacZ-Kan) in 1.5 mL eppendorf tubes and incubated 5h at 30˚C with
466 shaking (180 rpm), prior to serial dilution in PBS (Phosphate buffered saline) and
467 enumeration after overnight growth on LB media in the absence and presence of kanamycin.
468 Transformation frequency was calculated as the number of transformants divided by the
469 total number of bacteria.

470

Pilus shearing assay

Cultures were grown for 6h at 30˚C with shaking (180 rpm) in 25 mL LB + 0.2% arabinose within a 125 mL Erlenmeyer flask. To shear pili from the cell surface, 10 mL culture was removed, vortexed at max speed for 1 min, and cells removed by three sequential centrifugation steps (10min; 4000 x *g*; 4˚C). To the resulting supernatant saturated ammonium sulphate was added to 40% and incubated on ice for 1h. Precipitated proteins were recovered by centrifugation (30min; 20,000 x *g*; 4˚C) and washed once with PBS. Samples were then re-suspended in 2x Laemmli buffer, boiled (15min; 95˚C) and stored at -20˚C until needed. To compare PilA levels between samples the re-suspension volume was normalised according to the optical density of the starting culture. Total protein controls were intact cell lysates. The relative amount of PilA in each sample was determined by Western blotting.

Aggregation assay

Overnight cultures were back-diluted 1:100 in the absence and presence of arabinose, as needed, and grown in 14 mL round bottom polystyrene test tubes (Falcon, Corning) on a carousel style rotary wheel (40 rpm) at 30˚C. After 6h growth, aggregates were allowed to settle by standing the tube at RT for 30 min. The optical density at 600 nm ($O.D._{600}$) of the culture was then measured before and after mechanical disruption (vortex max speed; ~5 sec), which served to disperse any settled aggregates and return them to solution. Aggregation is expressed as the ratio of the $O.D._{600}$ Pre/Post-vortexing. For time-course experiments the standing time was reduced to 5 min. To visualise aggregates by microscopy overnight cultures were back-diluted either 1:100 individually or 1:200 when mixed, as needed, and were grown for 4h, as described above.

Microscopy

Cells were mounted on microscope slides coated with a thin agarose pad (1.2% w/v in PBS), covered with a #1 cover-slip, and were observed using a Zeiss Axio Imager M2 epi-fluorescence microscope attached to an AxioCam MRm camera and controlled by Zeiss AxioVision software. Image acquisition was done using a Plan-Apochromat 100×/1.4 Ph3 oil objective illuminated by an HXP120 lamp. Images were analysed and prepared for publication using ImageJ (http://rsb.info.nih.gov/ij).

Pilus staining and quantification

Alexa Fluor™ 488 C_5 Maleimide (AF-488-Mal; Thermo Fisher Scientific; Cat# A10254) was dissolved in DMSO, aliquoted and stored at -20˚C protected from light. Cultures used for staining were grown for 3.5h at 30˚C on the rotary wheel, as above, in the absence and presence of competence induction, as required. To stain cells 100 µL of culture was mixed with dye at a final concentration of 25 µg/mL[39] and incubated at RT for 5 min in the dark. Stained cells were harvested by centrifugation (5000 x *g*; 1 min), washed once with LB, re-suspended in 200 µL LB and imaged immediately. For quantification of piliation in snapshot imaging approximately 2000 cells per strain were analysed in each of three independent repeats. A subset of this data set was also analysed for the number of pili per cell and pilus length, as indicated in the text. For time-lapse analysis, images were acquired at RT at 10 sec intervals for 1 min (*i.e.* 7 frames). To analyse the number of pili produced per cell, per min, 5 fields of cells were analysed for each of the three independent repeats, yielding an analysis of 1947 cells in total.

Imaging on chitin surfaces

Visualisation of pilus production on chitin surfaces was done using chitin beads (NEB; Cat#S6651), which have previously been validated as a useful analogue for the natural chitin

surface[41,75]. Prior to use, chitin beads were washed 5x with 0.5x DASW + 50 mM HEPES + vitamins. Colonisation of chitin beads was done in 12-well culture plates (Cellstar) by mixing 0.1mL washed O/N culture with 0.1 mL washed beads in a final volume of 1 mL 0.5x DASW + 50 mM HEPES + vitamins, and incubated at 30˚C; 48h. Pilus staining was done as described above except that the final re-suspension volume was reduced to 50 µL. Stained beads were mounted directly on glass microscope slides, covered with a #1 cover-slip and imaged using either a Plan-Apochromat 100x/1.4 Ph3 or Plan-Neofluar 40x/1.3 Ph3 oil objective, as needed. To image cells after prolonged incubation (≥72h), plates were incubated within a homemade humidified chamber. To avoid damaging the beads manipulations were done using wide bore tips.

Western blotting

Cell lysates were prepared by suspending harvested cells in 2x Laemmli buffer (100 µL buffer per O.D. unit) before boiling at 95˚C for 15 min. Proteins were separated by SDS-PAGE using a 15% resolving gel and blotted onto PVDF membranes using a wet-transfer apparatus. Immuno-detection was performed as described previously[41]. Primary anti-PilA antibodies were raised in rabbits against synthetic peptides of A1552 PilA (Eurogentec, Belgium; #1510525) and used at a dilution of 1:5000. Anti-Rabbit IgG HRP (Sigma; Cat# A9169) diluted 1:5000 was used as a secondary antibody. Sample loading was verified with anti-RNA Sigma70-HRP (BioLegend; Cat# 663205) diluted 1:10,000.

Motility assay

To quantity motility phenotypes 2 µL overnight culture was spotted soft LB agar (0.3%) plates (two technical replicates) and incubated at RT for 24h prior to photography. The swarming diameter (cm) was measured and is expressed as the mean of three independent

biological repeats. A flagellin-deficient (Δ*flaA*) non-motile strain was used as a negative control.

Bioinformatics of PilA diversity

Vibrio cholerae genomes were obtained from NCBI (National Center for Biotechnology Information), and are listed in Supplementary File S1. Geneious software (10.2.3)[90] was used to perform custom BLAST analyses and identify *pilA*. Unique PilA sequences were extracted and combined with the PilA sequences from strain A1552 and a collection of environmental isolates, as deduced by Sanger sequencing (Supplementary File S2), as indicated in the text. PilA sequences were aligned with Muscle and a consensus neighbour-joining tree constructed using the Jukes-Cantor substitution model, resampled with 100 bootstrap replicates. MshA from strain A1552 was used as an outgroup.

Reproducibility

All data shown are representative of the results of at least three independent biological repeats.

Acknowledgements

We thank Ivan Mateus-Gonzalez for assistance with bioinformatics analyses. We further thank A. Boehm, S. Pukatzki, J. Mekalanos, and members of the Institut National de Recherche Biomédicale of the Democratic Republic of the Congo, for providing *V. cholerae* strains and V. Pelicic for advice on *pheS*-mediated counter-selection. Work on this problem was supported by a Marie Skłodowska-Curie Individual Fellowship (703340; CMDNAUP) to D.W.A. and by EPFL intramural funding and a Starting Grant from the European Research Council (ERC; 309064-VIR4ENV) to MB. M.B. is a Howard Hughes Medical Institute (HHMI) International Research Scholar (Grant# 55008726).

573

574 **Author contributions**

575 Conception, design and analysis: D.W.A and M.B. Performed research: D.W.A, S.S, C.S and

576 M.B. Wrote the manuscript: D.W.A and M.B.

577

578 **Declaration of Interests**

579 The authors declare no competing interests.

References

1 Maier, B. & Wong, G. C. L. How Bacteria Use Type IV Pili Machinery on Surfaces. *Trends in microbiology* **23**, 775-788, doi:10.1016/j.tim.2015.09.002 (2015).

2 Persat, A. *et al.* The mechanical world of bacteria. *Cell* **161**, 988-997, doi:10.1016/j.cell.2015.05.005 (2015).

3 Berry, J. L. & Pelicic, V. Exceptionally widespread nanomachines composed of type IV pilins: the prokaryotic Swiss Army knives. *FEMS microbiology reviews* **39**, 134-154, doi:10.1093/femsre/fuu001 (2015).

4 Giltner, C. L., Nguyen, Y. & Burrows, L. L. Type IV pilin proteins: versatile molecular modules. *Microbiology and molecular biology reviews : MMBR* **76**, 740-772, doi:10.1128/MMBR.00035-12 (2012).

5 Melville, S. & Craig, L. Type IV pili in Gram-positive bacteria. *Microbiology and molecular biology reviews : MMBR* **77**, 323-341, doi:10.1128/MMBR.00063-12 (2013).

6 Clemens, J. D., Nair, G. B., Ahmed, T., Qadri, F. & Holmgren, J. Cholera. *Lancet* **390**, 1539-1549, doi:10.1016/S0140-6736(17)30559-7 (2017).

7 Chang, Y. W. *et al.* Architecture of the *Vibrio cholerae* toxin-coregulated pilus machine revealed by electron cryotomography. *Nature microbiology* **2**, 16269, doi:10.1038/nmicrobiol.2016.269 (2017).

8 Chang, Y. W. *et al.* Architecture of the type IVa pilus machine. *Science* **351**, aad2001, doi:10.1126/science.aad2001 (2016).

9 Craig, L. *et al.* Type IV pilus structure by cryo-electron microscopy and crystallography: implications for pilus assembly and functions. *Molecular cell* **23**, 651-662, doi:10.1016/j.molcel.2006.07.004 (2006).

10 Gold, V. A., Salzer, R., Averhoff, B. & Kuhlbrandt, W. Structure of a type IV pilus machinery in the open and closed state. *eLife* **4**, doi:10.7554/eLife.07380 (2015).

11 Kolappan, S. *et al.* Structure of the *Neisseria meningitidis* Type IV pilus. *Nature communications* **7**, 13015, doi:10.1038/ncomms13015 (2016).

12 Merz, A. J., So, M. & Sheetz, M. P. Pilus retraction powers bacterial twitching motility. *Nature* **407**, 98-102, doi:10.1038/35024105 (2000).

13 Skerker, J. M. & Berg, H. C. Direct observation of extension and retraction of type IV pili. *Proceedings of the National Academy of Sciences of the United States of America* **98**, 6901-6904, doi:10.1073/pnas.121171698 (2001).

14 Jakovljevic, V., Leonardy, S., Hoppert, M. & Sogaard-Andersen, L. PilB and PilT are ATPases acting antagonistically in type IV pilus function in *Myxococcus xanthus*. *Journal of bacteriology* **190**, 2411-2421, doi:10.1128/JB.01793-07 (2008).

15 McCallum, M., Tammam, S., Khan, A., Burrows, L. L. & Howell, P. L. The molecular mechanism of the type IVa pilus motors. *Nature communications* **8**, 15091, doi:10.1038/ncomms15091 (2017).

16 Waldor, M. K. & Mekalanos, J. J. Lysogenic conversion by a filamentous phage encoding cholera toxin. *Science* **272**, 1910-1914 (1996).

17 Chiang, S. L., Taylor, R. K., Koomey, M. & Mekalanos, J. J. Single amino acid substitutions in the N-terminus of *Vibrio cholerae* TcpA affect colonization, autoagglutination, and serum resistance. *Molecular microbiology* **17**, 1133-1142 (1995).

18 Taylor, R. K., Miller, V. L., Furlong, D. B. & Mekalanos, J. J. Use of *phoA* gene fusions to identify a pilus colonization factor coordinately regulated with cholera toxin. *Proceedings of the National Academy of Sciences of the United States of America* **84**, 2833-2837 (1987).

19 Kirn, T. J., Lafferty, M. J., Sandoe, C. M. & Taylor, R. K. Delineation of pilin domains required for bacterial association into microcolonies and intestinal colonization by *Vibrio cholerae*. *Molecular microbiology* **35**, 896-910 (2000).

20 Chiavelli, D. A., Marsh, J. W. & Taylor, R. K. The mannose-sensitive hemagglutinin of *Vibrio cholerae* promotes adherence to zooplankton. *Applied and environmental microbiology* **67**, 3220-3225, doi:10.1128/AEM.67.7.3220-3225.2001 (2001).

21 Moorthy, S. & Watnick, P. I. Genetic evidence that the *Vibrio cholerae* monolayer is a distinct stage in biofilm development. *Molecular microbiology* **52**, 573-587, doi:10.1111/j.1365-2958.2004.04000.x (2004).

22 Utada, A. S. *et al. Vibrio cholerae* use pili and flagella synergistically to effect motility switching and conditional surface attachment. *Nature communications* **5**, 4913, doi:10.1038/ncomms5913 (2014).

23 Watnick, P. I., Fullner, K. J. & Kolter, R. A role for the mannose-sensitive hemagglutinin in biofilm formation by *Vibrio cholerae* El Tor. *Journal of bacteriology* **181**, 3606-3609 (1999).

24 Watnick, P. I. & Kolter, R. Steps in the development of a *Vibrio cholerae* El Tor biofilm. *Molecular microbiology* **34**, 586-595 (1999).

25 Tamplin, M. L., Gauzens, A. L., Huq, A., Sack, D. A. & Colwell, R. R. Attachment of *Vibrio cholerae* serogroup O1 to zooplankton and phytoplankton of Bangladesh waters. *Applied and environmental microbiology* **56**, 1977-1980 (1990).

26 Blokesch, M. Competence-induced type VI secretion might foster intestinal colonization by *Vibrio cholerae*: Intestinal interbacterial killing by competence-induced *V. cholerae*. *BioEssays : news and reviews in molecular, cellular and developmental biology* **37**, 1163-1168, doi:10.1002/bies.201500101 (2015).

27 Colwell, R. R. *et al.* Reduction of cholera in Bangladeshi villages by simple filtration. *Proceedings of the National Academy of Sciences of the United States of America* **100**, 1051-1055, doi:10.1073/pnas.0237386100 (2003).

28 Huq, A. *et al.* A simple filtration method to remove plankton-associated *Vibrio cholerae* in raw water supplies in developing countries. *Applied and environmental microbiology* **62**, 2508-2512 (1996).

29 Meibom, K. L. *et al.* The *Vibrio cholerae* chitin utilization program. *Proceedings of the National Academy of Sciences of the United States of America* **101**, 2524-2529 (2004).

30 Meibom, K. L., Blokesch, M., Dolganov, N. A., Wu, C. Y. & Schoolnik, G. K. Chitin induces natural competence in *Vibrio cholerae*. *Science* **310**, 1824-1827, doi:10.1126/science.1120096 (2005).

31 Johnston, C., Martin, B., Fichant, G., Polard, P. & Claverys, J. P. Bacterial transformation: distribution, shared mechanisms and divergent control. *Nature reviews. Microbiology* **12**, 181-196, doi:10.1038/nrmicro3199 (2014).

32 Seitz, P. & Blokesch, M. DNA-uptake machinery of naturally competent *Vibrio cholerae*. *Proceedings of the National Academy of Sciences of the United States of America* **110**, 17987-17992, doi:10.1073/pnas.1315647110 (2013).

33 Seitz, P. *et al.* ComEA is essential for the transfer of external DNA into the periplasm in naturally transformable *Vibrio cholerae* cells. *PLoS genetics* **10**, e1004066, doi:10.1371/journal.pgen.1004066 (2014).

34 Seitz, P. & Blokesch, M. DNA transport across the outer and inner membranes of naturally transformable *Vibrio cholerae* is spatially but not temporally coupled. *mBio* **5**, doi:10.1128/mBio.01409-14 (2014).

35 Wolfgang, M. *et al.* PilT mutations lead to simultaneous defects in competence for natural transformation and twitching motility in piliated *Neisseria gonorrhoeae*. *Molecular microbiology* **29**, 321-330 (1998).

36 Draskovic, I. & Dubnau, D. Biogenesis of a putative channel protein, ComEC, required for DNA uptake: membrane topology, oligomerization and formation of disulphide bonds. *Molecular microbiology* **55**, 881-896, doi:10.1111/j.1365-2958.2004.04430.x (2005).

37 Gangel, H. *et al.* Concerted spatio-temporal dynamics of imported DNA and ComE DNA uptake protein during gonococcal transformation. *PLoS pathogens* **10**, e1004043, doi:10.1371/journal.ppat.1004043 (2014).

38 Laurenceau, R. *et al.* A type IV pilus mediates DNA binding during natural transformation in *Streptococcus pneumoniae*. *PLoS pathogens* **9**, e1003473, doi:10.1371/journal.ppat.1003473 (2013).

39 Ellison, C. K. *et al.* Obstruction of pilus retraction stimulates bacterial surface sensing. *Science* **358**, 535-538, doi:10.1126/science.aan5706 (2017).

40 Blair, K. M., Turner, L., Winkelman, J. T., Berg, H. C. & Kearns, D. B. A molecular clutch disables flagella in the *Bacillus subtilis* biofilm. *Science* **320**, 1636-1638, doi:10.1126/science.1157877 (2008).

41 Lo Scrudato, M. & Blokesch, M. The regulatory network of natural competence and transformation of *Vibrio cholerae*. *PLoS genetics* **8**, e1002778, doi:10.1371/journal.pgen.1002778 (2012).

42 Metzger, L. C. & Blokesch, M. Composition of the DNA-uptake complex of *Vibrio cholerae*. *Mobile genetic elements* **4**, e28142, doi:10.4161/mge.28142 (2014).

43 Jones, C. J. *et al.* C-di-GMP Regulates Motile to Sessile Transition by Modulating MshA Pili Biogenesis and Near-Surface Motility Behavior in *Vibrio cholerae*. *PLoS pathogens* **11**, e1005068, doi:10.1371/journal.ppat.1005068 (2015).

44 Fong, J. C., Syed, K. A., Klose, K. E. & Yildiz, F. H. Role of Vibrio polysaccharide (vps) genes in VPS production, biofilm formation and *Vibrio cholerae* pathogenesis. *Microbiology* **156**, 2757-2769, doi:10.1099/mic.0.040196-0 (2010).

45 Absalon, C., Van Dellen, K. & Watnick, P. I. A communal bacterial adhesin anchors biofilm and bystander cells to surfaces. *PLoS pathogens* **7**, e1002210, doi:10.1371/journal.ppat.1002210 (2011).

46 Berk, V. *et al.* Molecular architecture and assembly principles of *Vibrio cholerae* biofilms. *Science* **337**, 236-239, doi:10.1126/science.1222981 (2012).

47 Kirn, T. J., Jude, B. A. & Taylor, R. K. A colonization factor links *Vibrio cholerae* environmental survival and human infection. *Nature* **438**, 863-866, doi:10.1038/nature04249 (2005).

48 Bartlett, T. M. *et al.* A Periplasmic Polymer Curves *Vibrio cholerae* and Promotes Pathogenesis. *Cell* **168**, 172-185 e115, doi:10.1016/j.cell.2016.12.019 (2017).

49 Gebhart, C. *et al.* Characterization of exogenous bacterial oligosaccharyltransferases in *Escherichia coli* reveals the potential for O-linked protein glycosylation in *Vibrio cholerae* and *Burkholderia thailandensis*. *Glycobiology* **22**, 962-974, doi:10.1093/glycob/cws059 (2012).

50 Biais, N., Ladoux, B., Higashi, D., So, M. & Sheetz, M. Cooperative retraction of bundled type IV pili enables nanonewton force generation. *PLoS biology* **6**, e87, doi:10.1371/journal.pbio.0060087 (2008).

51 Joelsson, A., Liu, Z. & Zhu, J. Genetic and phenotypic diversity of quorum-sensing systems in clinical and environmental isolates of *Vibrio cholerae*. *Infection and immunity* **74**, 1141-1147, doi:10.1128/IAI.74.2.1141-1147.2006 (2006).

52 Aagesen, A. M. & Häse, C. C. Sequence analyses of type IV pili from *Vibrio cholerae*, *Vibrio parahaemolyticus*, and *Vibrio vulnificus*. *Microbial ecology* **64**, 509-524, doi:10.1007/s00248-012-0021-2 (2012).

53 Aldova, E., Laznickova, K., Stepankova, E. & Lietava, J. Isolation of nonagglutinable vibrios from an enteritis outbreak in Czechoslovakia. *The Journal of infectious diseases* **118**, 25-31 (1968).

54 Chun, J. *et al.* Comparative genomics reveals mechanism for short-term and long-term clonal transitions in pandemic *Vibrio cholerae*. *Proceedings of the National Academy of Sciences of the United States of America* **106**, 15442-15447, doi:10.1073/pnas.0907787106 (2009).

55 Blokesch, M. & Schoolnik, G. K. Serogroup conversion of *Vibrio cholerae* in aquatic reservoirs. *PLoS pathogens* **3**, e81, doi:10.1371/journal.ppat.0030081 (2007).

56 Li, M., Shimada, T., Morris, J. G., Jr., Sulakvelidze, A. & Sozhamannan, S. Evidence for the emergence of non-O1 and non-O139 *Vibrio cholerae* strains with pathogenic potential by exchange of O-antigen biosynthesis regions. *Infection and immunity* **70**, 2441-2453 (2002).

57 DiRita, V. J., Neely, M., Taylor, R. K. & Bruss, P. M. Differential expression of the ToxR regulon in classical and E1 Tor biotypes of *Vibrio cholerae* is due to biotype-specific control over toxT expression. *Proceedings of the National Academy of Sciences of the United States of America* **93**, 7991-7995 (1996).

58 Jude, B. A. & Taylor, R. K. The physical basis of type 4 pilus-mediated microcolony formation by *Vibrio cholerae* O1. *Journal of structural biology* **175**, 1-9, doi:10.1016/j.jsb.2011.04.008 (2011).

59 Lim, M. S. *et al. Vibrio cholerae* El Tor TcpA crystal structure and mechanism for pilus-mediated microcolony formation. *Molecular microbiology* **77**, 755-770, doi:10.1111/j.1365-2958.2010.07244.x (2010).

60 Rhine, J. A. & Taylor, R. K. TcpA pilin sequences and colonization requirements for O1 and O139 *Vibrio cholerae*. *Molecular microbiology* **13**, 1013-1020 (1994).

61 Ellison, C. K. *et al.* Retraction of DNA-bound type IV competence pili initiates DNA uptake during natural transformation in *Vibrio cholerae*. *Nature microbiology* **3**, 773-780, doi:10.1038/s41564-018-0174-y (2018).

62 Hélaine, S. *et al.* PilX, a pilus-associated protein essential for bacterial aggregation, is a key to pilus-facilitated attachment of *Neisseria meningitidis* to human cells. *Molecular microbiology* **55**, 65-77, doi:10.1111/j.1365-2958.2004.04372.x (2005).

63 Imhaus, A. F. & Duménil, G. The number of *Neisseria meningitidis* type IV pili determines host cell interaction. *The EMBO journal* **33**, 1767-1783, doi:10.15252/embj.201488031 (2014).

64 Nielsen, A. T. *et al.* A bistable switch and anatomical site control *Vibrio cholerae* virulence gene expression in the intestine. *PLoS pathogens* **6**, e1001102, doi:10.1371/journal.ppat.1001102 (2010).

65 Krebs, S. J. & Taylor, R. K. Protection and attachment of *Vibrio cholerae* mediated by the toxin-coregulated pilus in the infant mouse model. *Journal of bacteriology* **193**, 5260-5270, doi:10.1128/JB.00378-11 (2011).

66 Shime-Hattori, A. *et al.* Two type IV pili of *Vibrio parahaemolyticus* play different roles in biofilm formation. *FEMS microbiology letters* **264**, 89-97, doi:10.1111/j.1574-6968.2006.00438.x (2006).

67 Hang, L. *et al.* Use of in vivo-induced antigen technology (IVIAT) to identify genes uniquely expressed during human infection with *Vibrio cholerae*. *Proceedings of the National Academy of Sciences of the United States of America* **100**, 8508-8513, doi:10.1073/pnas.1431769100 (2003).

68 Oldewurtel, E. R., Kouzel, N., Dewenter, L., Henseler, K. & Maier, B. Differential interaction forces govern bacterial sorting in early biofilms. *eLife* **4**, doi:10.7554/eLife.10811 (2015).

69 Chamot-Rooke, J. *et al.* Posttranslational modification of pili upon cell contact triggers *N. meningitidis* dissemination. *Science* **331**, 778-782, doi:10.1126/science.1200729 (2011).

70 Smukalla, S. *et al.* FLO1 is a variable green beard gene that drives biofilm-like cooperation in budding yeast. *Cell* **135**, 726-737, doi:10.1016/j.cell.2008.09.037 (2008).

71 Hirose, S., Benabentos, R., Ho, H. I., Kuspa, A. & Shaulsky, G. Self-recognition in social amoebae is mediated by allelic pairs of tiger genes. *Science* **333**, 467-470, doi:10.1126/science.1203903 (2011).

72 Pathak, D. T., Wei, X., Dey, A. & Wall, D. Molecular recognition by a polymorphic cell surface receptor governs cooperative behaviors in bacteria. *PLoS genetics* **9**, e1003891, doi:10.1371/journal.pgen.1003891 (2013).

73 Strassmann, J. E., Gilbert, O. M. & Queller, D. C. Kin discrimination and cooperation in microbes. *Annual review of microbiology* **65**, 349-367, doi:10.1146/annurev.micro.112408.134109 (2011).

74 Wall, D. Kin Recognition in Bacteria. *Annual review of microbiology* **70**, 143-160, doi:10.1146/annurev-micro-102215-095325 (2016).

75 Borgeaud, S., Metzger, L. C., Scrignari, T. & Blokesch, M. The type VI secretion system of *Vibrio cholerae* fosters horizontal gene transfer. *Science* **347**, 63-67, doi:10.1126/science.1260064 (2015).

76 Ho, B. T., Dong, T. G. & Mekalanos, J. J. A view to a kill: the bacterial type VI secretion system. *Cell host & microbe* **15**, 9-21, doi:10.1016/j.chom.2013.11.008 (2014).

77 Trunk, T., Khalil, H. S. & Leo, J. C. Bacterial autoaggregation. *AIMS Microbiology* **4**, 140-164, doi:http://dx.doi.org/10.3934/microbiol.2018.1.140 (2018).

78 Yildiz, F. H. & Schoolnik, G. K. Role of *rpoS* in stress survival and virulence of *Vibrio cholerae*. *Journal of bacteriology* **180**, 773-784 (1998).

79 Blokesch, M. A quorum sensing-mediated switch contributes to natural transformation of *Vibrio cholerae*. *Mobile genetic elements* **2**, 224-227, doi:10.4161/mge.22284 (2012).

80 Sambrook, J., Fritsch, E. F. & Maniatis, T. Molecular Cloning: A Laboratory Manual. *Cold Spring Harbor: Cold Spring Harbor Laboratory Press* (1989).

81 De Souza Silva, O. & Blokesch, M. Genetic manipulation of *Vibrio cholerae* by combining natural transformation with FLP recombination. *Plasmid* **64**, 186-195, doi:10.1016/j.plasmid.2010.08.001 (2010).

82 Marvig, R. L. & Blokesch, M. Natural transformation of *Vibrio cholerae* as a tool - optimizing the procedure. *BMC microbiology* **10**, 155, doi:10.1186/1471-2180-10-155 (2010).

83 Van der Henst, C. *et al.* Molecular insights into *Vibrio cholerae*'s intra-amoebal host-pathogen interactions. *Nature communications*, doi:10.1038/s41467-018-05976-x (2018).

84 Gurung, I., Berry, J. L., Hall, A. M. J. & Pelicic, V. Cloning-independent markerless gene editing in *Streptococcus sanguinis*: novel insights in type IV pilus biology. *Nucleic acids research* **45**, e40, doi:10.1093/nar/gkw1177 (2017).

85 Bao, Y., Lies, D. P., Fu, H. & Roberts, G. P. An improved Tn7-based system for the single-copy insertion of cloned genes into chromosomes of gram-negative bacteria. *Gene* **109**, 167-168 (1991).

86 Yamamoto, S. *et al.* Regulation of natural competence by the orphan two-component system sensor kinase ChiS involves a non-canonical transmembrane regulator in *Vibrio cholerae*. *Molecular microbiology* **91**, 326-347, doi:10.1111/mmi.12462 (2014).

87 Dalia, A. B., Lazinski, D. W. & Camilli, A. Identification of a membrane-bound transcriptional regulator that links chitin and natural competence in Vibrio cholerae. *mBio* **5**, e01028-01013, doi:10.1128/mBio.01028-13 (2014).

88 Yamamoto, S. *et al.* Identification of a chitin-induced small RNA that regulates translation of the tfoX gene, encoding a positive regulator of natural competence in Vibrio cholerae. *Journal of bacteriology* **193**, 1953-1965, doi:10.1128/JB.01340-10 (2011).

89 Lo Scrudato, M. & Blokesch, M. A transcriptional regulator linking quorum sensing and chitin induction to render *Vibrio cholerae* naturally transformable. *Nucleic acids research* **41**, 3644-3658, doi:10.1093/nar/gkt041 (2013).

90 Kearse, M. *et al.* Geneious Basic: an integrated and extendable desktop software platform for the organization and analysis of sequence data. *Bioinformatics* **28**, 1647-1649, doi:10.1093/bioinformatics/bts199 (2012).

Figure 1

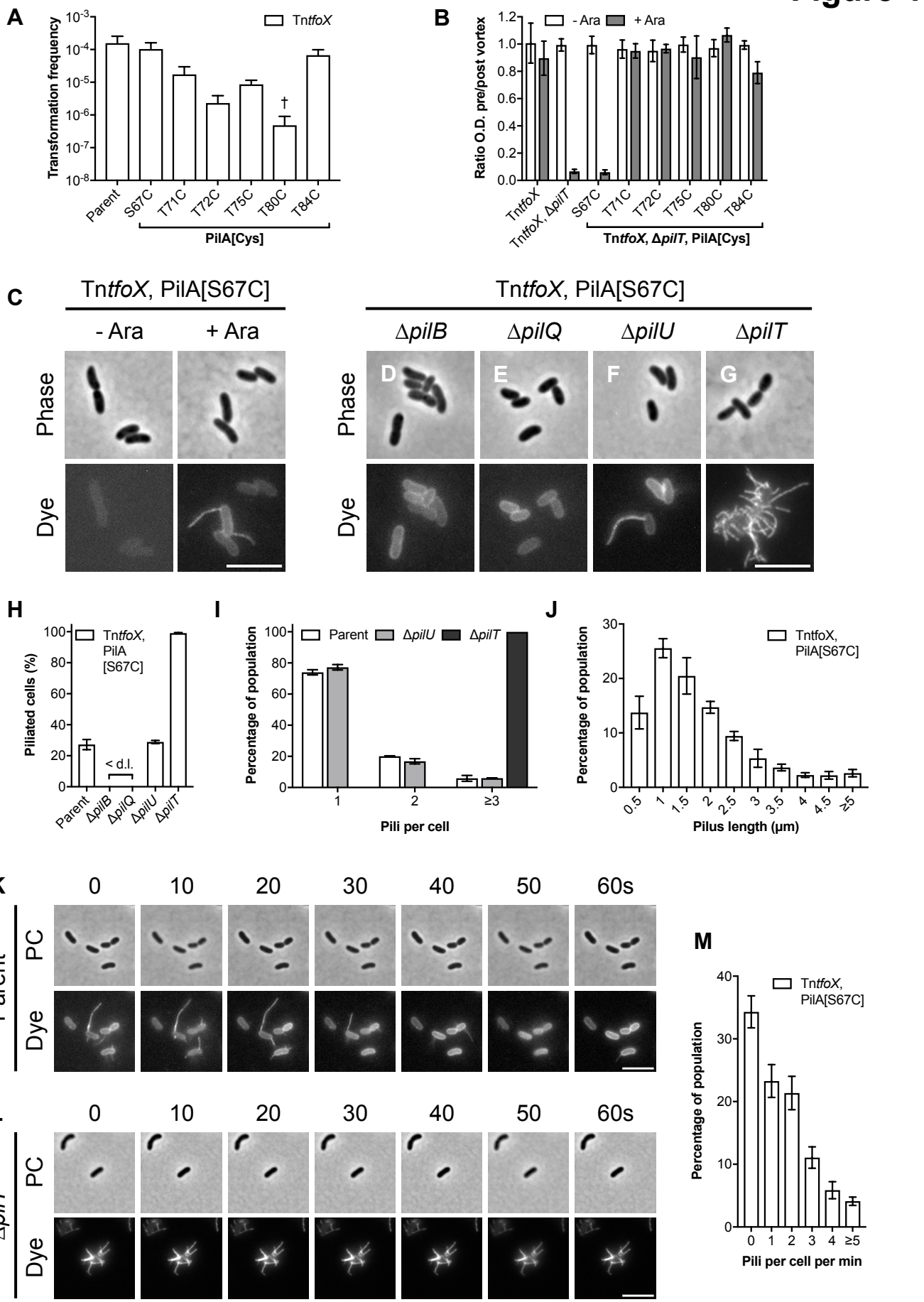

Figure 1. Direct observation of dynamic DNA-uptake pili.

(**A**) Functionality of PilA cysteine variants (PilA[Cys]) in a chitin-independent transformation assay using strains carrying an arabinose-inducible copy of *tfoX* (Tn*tfoX*). Transformation frequencies are the mean of three independent biological repeats (+S.D.). < d.l., below detection limit. †, < d.l. in one repeat.

(**B**) Effect of PilA cysteine variants on the ability of retraction deficient (Tn*tfoX*, Δ*pilT*) cells to aggregate. Aggregation is shown as the ratio of the culture optical density ($O.D._{600}$) before and after vortexing, in the absence (- Ara) and presence (+ Ara) of *tfoX* induction, as indicated. Values are the mean of three independent biological repeats (±S.D.).

(**C**-**G**) Snapshot imaging of pili in cells of A1552-Tn*tfoX*, PilA[S67C] and its derivatives. (**C**) Cells of A1552-Tn*tfoX*, PilA[S67C] were grown in the absence (- Ara) and presence (+ Ara) of *tfoX* induction, as indicated, and stained with AF-488-Mal. Bar = 5 µm. (D-E) Cells of A1552-Tn*tfoX*, PilA[S67C] were grown in the presence of *tfoX* induction and stained with AF-488-Mal in a (**D**) Δ*pilB*, (**E**) Δ*pilQ*, (**F**) Δ*pilU* and (**G**) Δ*pilT* background, as indicated. Bar = 5 µm.

(**H**-**J**) Quantification of piliation in snapshot imaging. Bars represent the mean of three repeats (±S.D.). (**H**) Percentage of piliated cells in the indicated backgrounds. *n* = *c.a.* 2000 cells per strain per repeat. (**I**) Histogram of number of pili per cell in piliated cells in WT parent (A1552-Tn*tfoX*, PilA[S67C]), Δ*pilU* (A1552-Tn*tfoX*, PilA[S67C], Δ*pilU*) and Δ*pilT* (A1552-Tn*tfoX*, PilA[S67C], Δ*pilT*) backgrounds, as indicated. *n* = *c.a.* 300 cells per strain per repeat. (**J**) Histogram of pilus length in cells of A1552-Tn*tfoX*, PilA[S67C]. *n* = *c.a.* 500-600 cells per repeat.

(**K**-**L**) Time-lapse series of pilus dynamics in (**K**) WT parent (A1552-Tn*tfoX*, PilA[S67C]) and (**L**) Δ*pilT* (A1552-Tn*tfoX*, PilA[S67C], Δ*pilT*) backgrounds. Cells were stained with AF-488-Mal and imaged at 10s intervals for 1 minute. Upper panels show phase-contrast (PC), lower panels show fluorescence (dye). Time in seconds (s), as indicated. Bars = 5 µm.

(**M**) Histogram showing quantification of pili produced per cell per min in the WT parent (A1552-Tn*tfoX*, PilA[S67C]) background. Bars represent the mean of three repeats (±S.D.). *n* = *c.a.* 500-700 cells per repeat.

Figure 2

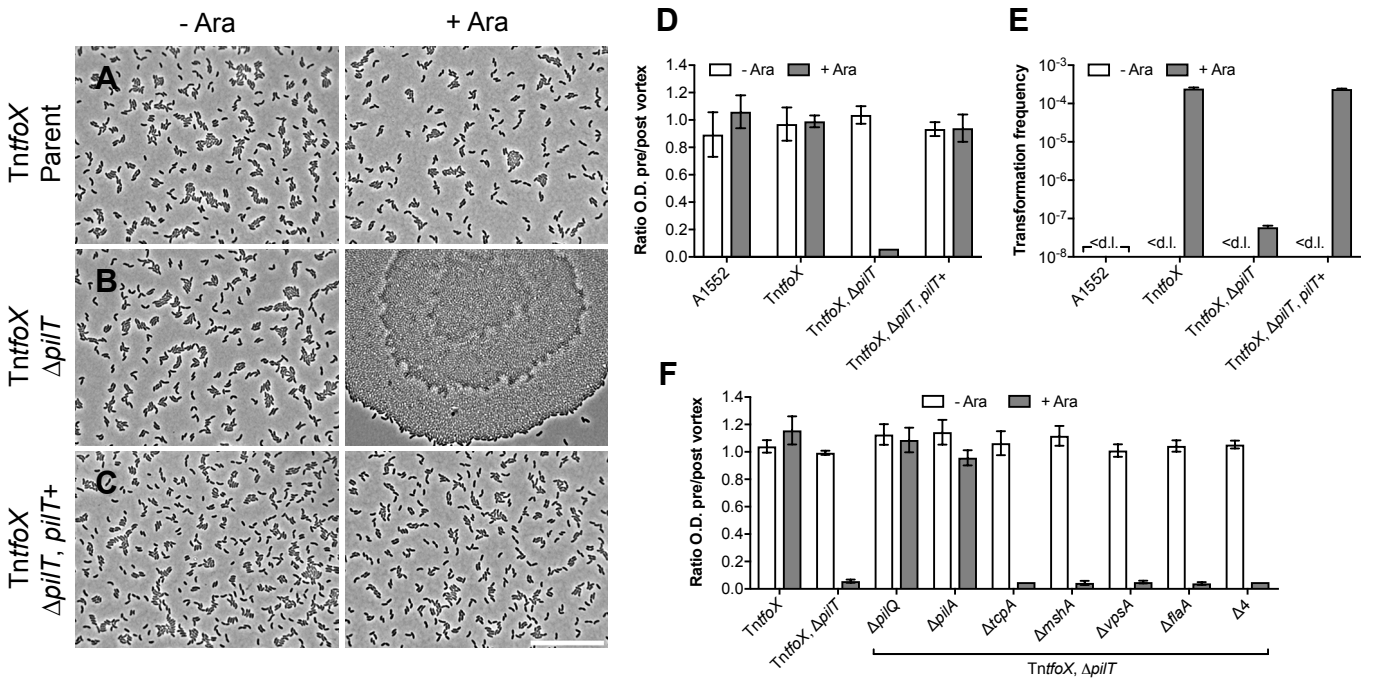

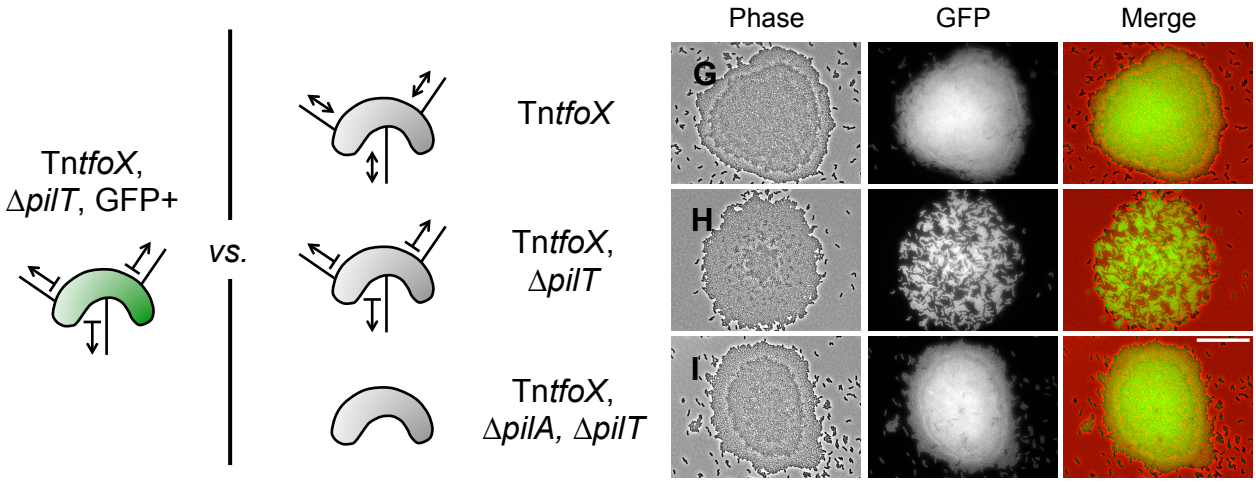

Figure 2. Competent cells auto-aggregate in the absence of pilus retraction.

(**A**-**C**) Phase-contrast microscopy of cells of strains (**A**) A1552-Tn*tfoX*, (**B**) A1552-Tn*tfoX*, Δ*pilT* and (**C**) A1552-Tn*tfoX*, Δ*pilT*, *pilT*+, grown in the absence (- Ara) and presence (+ Ara) of *tfoX* induction, as indicated. Scale bar = 25 μm.

(**D**-**E**) Aggregation and transformation frequency of cells of strains A1552-Tn*tfoX*, A1552-Tn*tfoX*, Δ*pilT* and A1552-Tn*tfoX*, Δ*pilT*, *pilT*+, grown in the absence (- Ara) and presence (+ Ara) of *tfoX* induction, as indicated. A1552 (without inducible *tfoX*) was used as a negative control. (**D**) Aggregation is shown as the ratio of the culture optical density ($O.D._{600}$) before and after vortexing. Values are the mean of three repeats (±S.D.). (**E**) Chitin-independent transformation frequency assay. Values are the mean of three repeats (+S.D.). < d.l., below detection limit.

(**F**) Effect of various deletion backgrounds on the ability of retraction deficient cells to aggregate. Aggregation is shown as the ratio of the culture optical density ($O.D._{600}$) before and after vortexing, in the absence (- Ara) and presence (+ Ara) of *tfoX* induction, as indicated. Δ4 = Δ*tcpA*, Δ*mshA*, Δ*vpsA*, Δ*flaA* quadruple mutant. Values are the mean of three repeats (±S.D.).

(**G**-**I**) Co-culture of fluorescent Δ*pilT* cells (A1552-Tn*tfoX*, Δ*pilT*, GFP+) producing GFP and non-fluorescent cells of the (**G**) WT parent (A1552-Tn*tfoX*), (**H**) Δ*pilT* (A1552-Tn*tfoX*, Δ*pilT*) and (**I**) Δ*pilA*, Δ*pilT* (A1552-Tn*tfoX*, Δ*pilA*, Δ*pilT*), grown in the presence of *tfoX* induction. Merged images show GFP in green and phase-contrast in red. Bar = 25 μm.

Figure 3

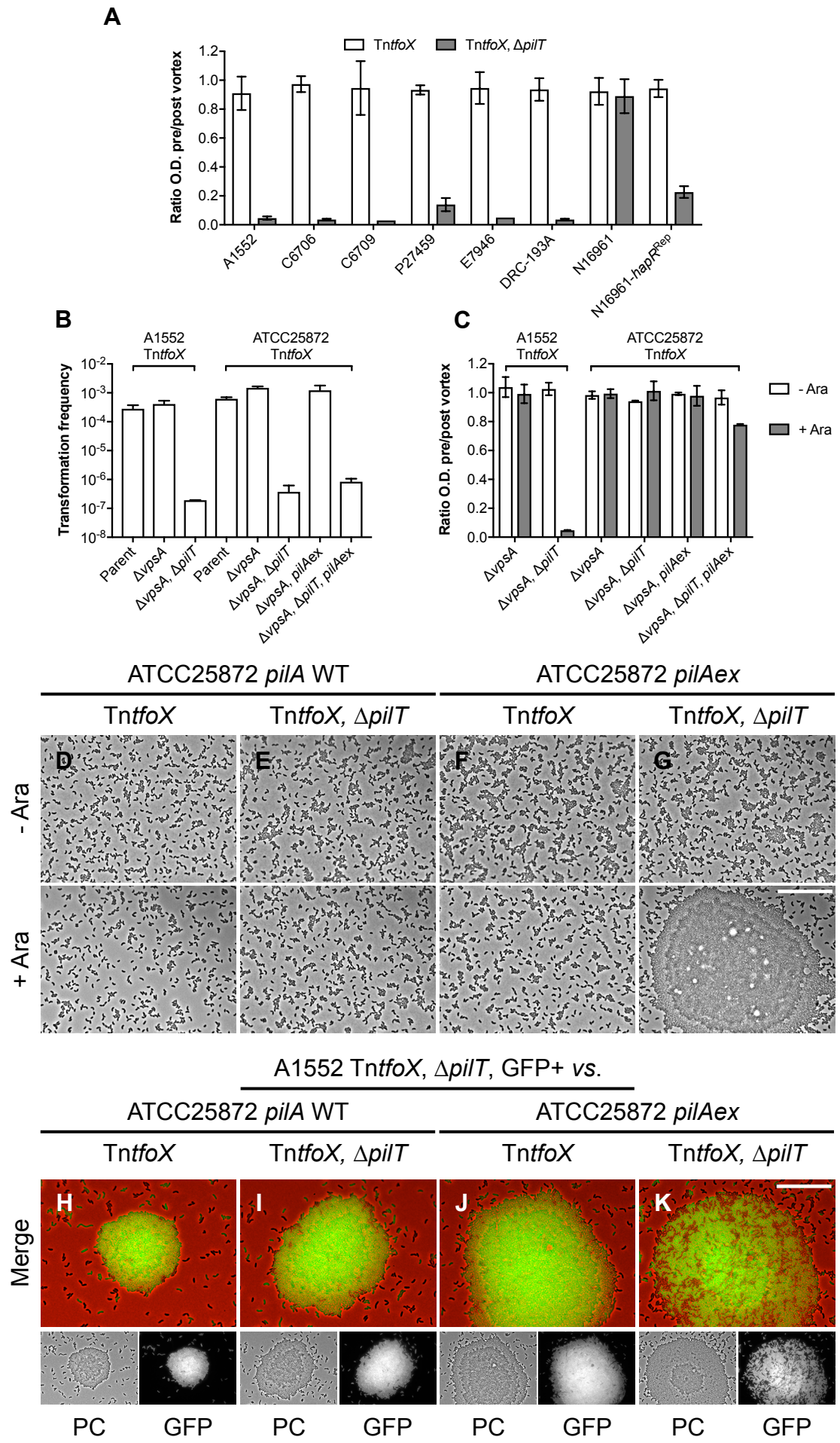

Figure 3. A1552 PilA is sufficient for aggregation in a non-pandemic strain.

(**A**) Aggregation of representative 7th pandemic strains of *V. cholerae*, including the effect of *hapR*^{Rep} on N16961, in a Tn*tfoX* and a Tn*tfoX*, Δ*pilT* background, as indicated. Aggregation is shown as the ratio of the culture optical density (O.D. $_{600}$) before and after vortexing, in the presence of *tfoX* induction. Values are the mean of three repeats (±S.D.).

(**B**-**C**) Transformation frequency and aggregation of *V. cholerae* strain ATCC25872-Tn*tfoX* compared to that of A1552-Tn*tfoX*. (**B**) Chitin-independent transformation assay. Transformation frequencies are the mean of three repeats (+S.D.). (**C**) Aggregation is shown as the ratio of the culture optical density (O.D. $_{600}$) before and after vortexing, in the absence (- Ara) and presence (+ Ara) of *tfoX* induction, as indicated. Values are the mean of three repeats (±S.D.).

(**D**-**G**) Phase-contrast microscopy of ATCC25872-Tn*tfoX*, Δ*vpsA* cells carrying (**D** and **E**) their native *pilA* (*pilA* WT) and (**F** and **G**) A1552 *pilA* (*pilA*ex), in a (**D** and **F**) *pilT*+ and (**E** and **G**) Δ*pilT* background, as indicated. Strains were cultured in the absence (- Ara) and presence (+ Ara), as indicated. Bar = 25 µm. Note that ATCC25872 derivatives were co-deleted for *vpsA* to rule out any compounding effects of biofilm formation.

(**H**-**K**) Co-culture of fluorescent cells of A1552-Tn*tfoX*, Δ*pilT*, GFP+, producing GFP, and non-fluorescent cells of ATCC25872-Tn*tfoX*, Δ*vpsA* carrying (**H** and **I**) their native *pilA* (*pilA* WT) and (**J** and **K**) A1552 PilA (*pilA*ex), in a (**H** and **J**) *pilT*+ and (**I** and **K**) Δ*pilT* background, as indicated. Cells were grown in the presence of *tfoX* induction. Merged images show GFP in green and phase-contrast (PC) in red. Bar = 25 µm.

Figure 4

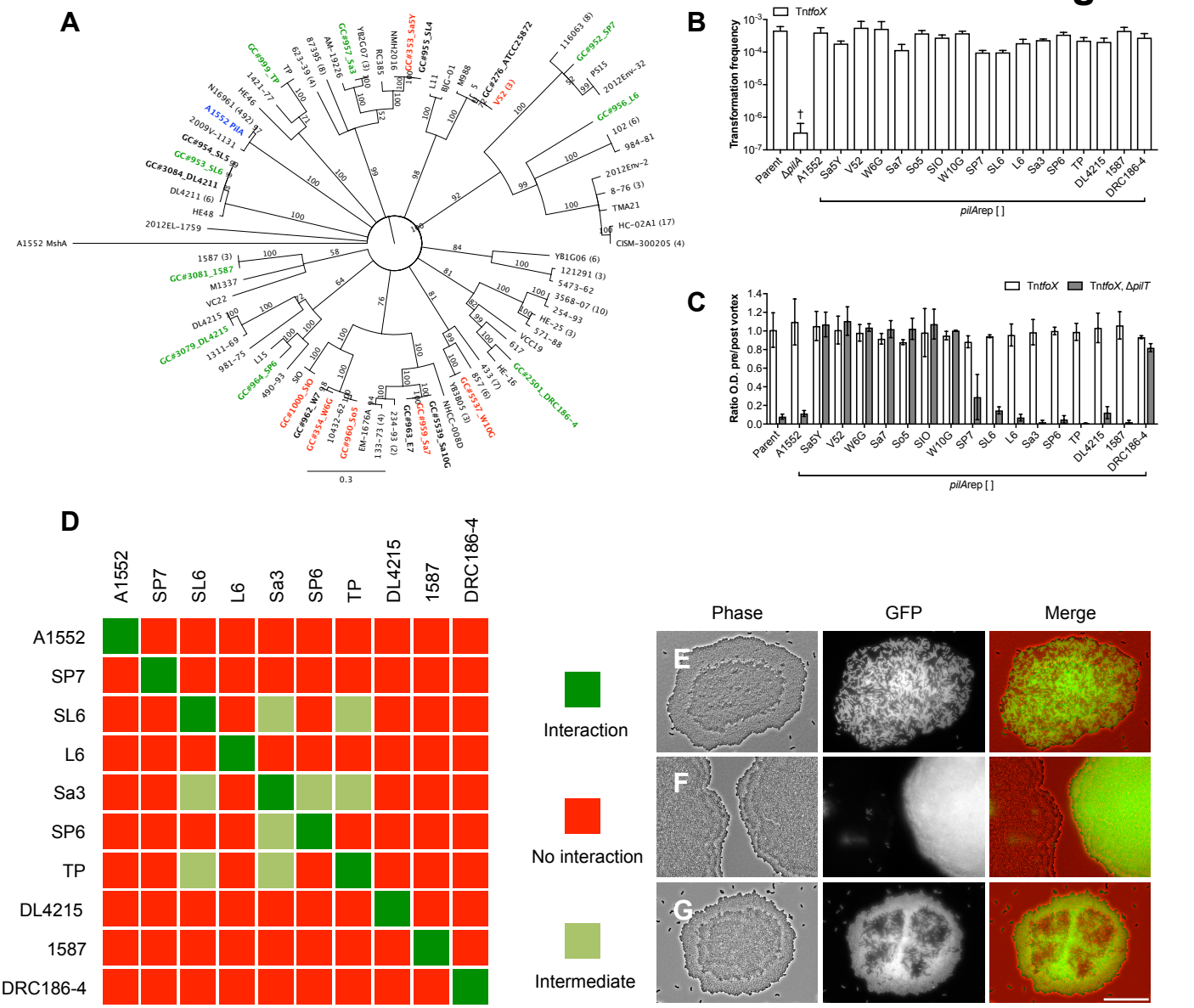

Figure 4. PilA variability governs auto-aggregation and enables kin-recognition.

(**A**) Consensus neighbour-joining phylogenetic tree of PilA. The tree consists of the 56 unique PilA sequences identified from NCBI, 22 sequences from an in-house collection of various environmental and patient isolates (bold), and A1552 PilA (blue) and MshA (outgroup). Values shown are consensus support values (%). Aggregation capable (green) and incapable (red) PilAs tested in the *pilA*rep experiments are highlighted. Note that ATCC25872 and V52 PilA are identical.

(**B**-**C**) Functionality of A1552-Tn*tfoX*, *pilA*rep[A1552] and 16 different PilAs assessed by transformation frequency and aggregation. (**B**) Chitin-independent transformation frequency assay. WT parent (A1552-Tn*tfoX*) and Δ*pilA* (A1552-Tn*tfoX*, Δ*pilA*) strains served as positive and negative controls. Transformation frequencies are the mean of three repeats (+S.D.). †, <d.l. in one repeat. (**C**) Aggregation was determined for the WT parent and each *pilA*rep strain in a *pilT*+ (A1552-Tn*tfoX*) and Δ*pilT* (A1552-Tn*tfoX*, Δ*pilT*) background, as indicated. Aggregation is shown as the ratio of the culture optical density (O.D. $_{600}$) before and after vortexing, in the presence of *tfoX* induction. Values are the mean of three repeats (±S.D.).

(**D**) Interaction matrix showing the results of a pairwise analysis of all possible interactions between aggregation proficient PilA. Interactions were tested by co-culturing non-fluorescent cells of the relevant Tn*tfoX*, Δ*pilT*, pilA*rep*[] strains with a fluorescent (GFP+) derivative of each strain. Cells were grown in the presence of *tfoX* induction. Self-self combinations served as controls.

(**E**-**G**) Representative examples of (**E**) interaction, resulting in well-mixed aggregates (**F**) no interaction, resulting in fluorescent or non-fluorescent aggregates and (**G**) intermediate interactions, resulting in patterned aggregates. Cells were grown in the presence of *tfoX* induction. Merged images show GFP in green and phase-contrast (PC) in red. Bar = 25 µm.

Figure 5

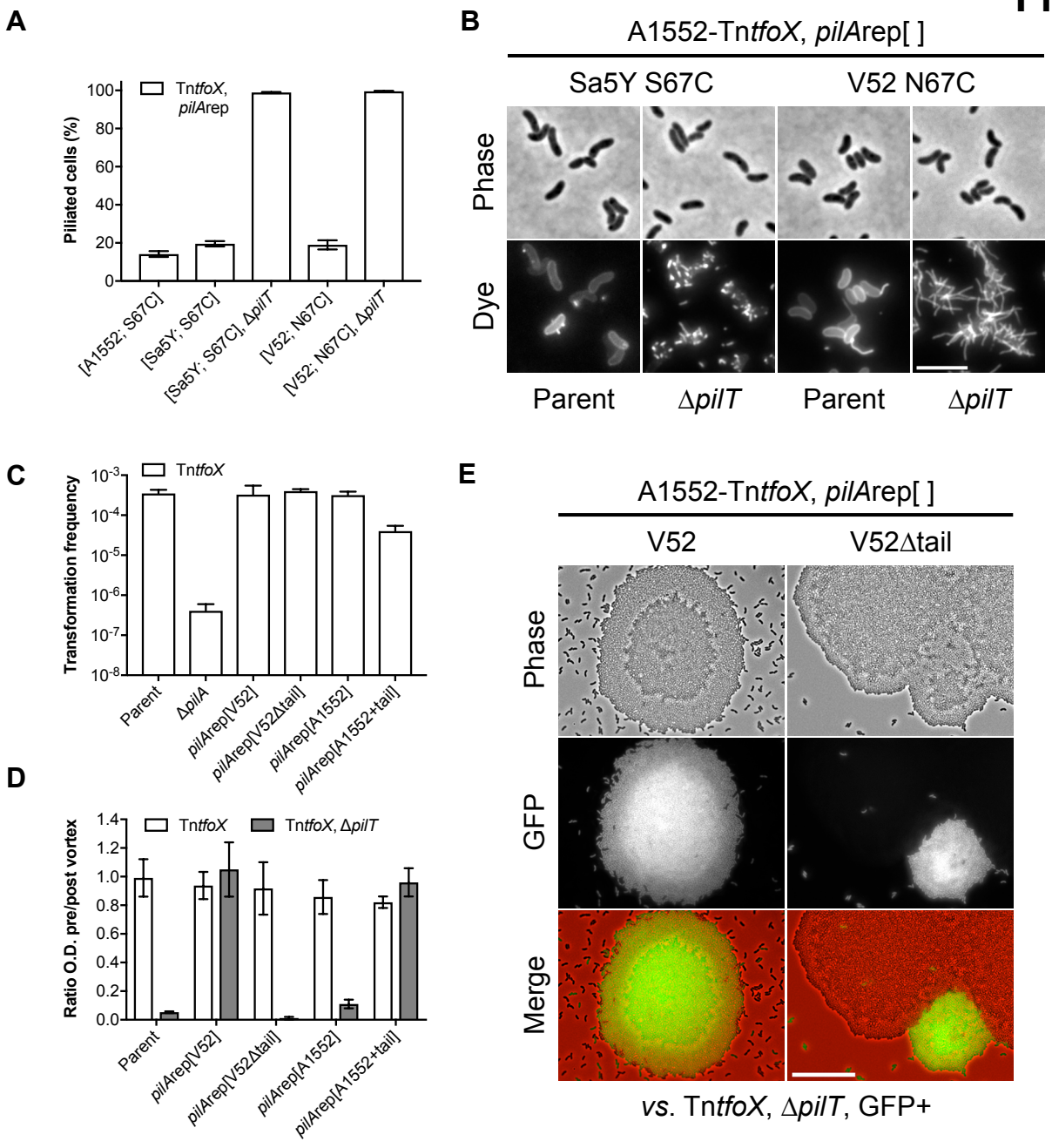

Figure 5. The unusual tail of ATCC25872/V52 PilA inhibits aggregation.

(**A**) Quantification of piliation in snapshot imaging of cells of strains A1552-Tn*tfoX*, *pilA*rep[A1552; S67C], A1552-Tn*tfoX*, *pilA*rep[Sa5Y; S67C] and A1552-Tn*tfoX*, *pilA*rep[V52; N67C], in the indicated backgrounds. Cells were grown with *tfoX* induction and pili stained with AF-488-Mal. Bars represent the mean of three repeats (±S.D.). *n* = *c.a.* 2000 cells per strain per repeat. (**B**) Direct observation of pili stained with AF-488-Mal in cells carrying *pilA*rep[Sa5Y; S67C] and *pilA*rep[V52; N67C], in a WT parent (A1552-Tn*tfoX*) and Δ*pilT* (A1552-Tn*tfoX*, Δ*pilT*) background, as indicated. Bar = 5 µm.

(**C**-**D**) Functionality of *pilA*rep tail variants assessed by natural transformation and aggregation. (**C**) Chitin-independent transformation assay. WT parent (A1552-Tn*tfoX*) and Δ*pilA* (A1552-Tn*tfoX*, Δ*pilA*) strains served as positive and negative controls. Transformation frequencies are the mean of three repeats (+S.D.). (**D**) Aggregation was determined for the WT parent and each *pilA*rep strain in a *pilT*+ (A1552-Tn*tfoX*) and Δ*pilT* (A1552-Tn*tfoX*, Δ*pilT*) background, as indicated. Aggregation is shown as the ratio of the culture optical density ($O.D._{600}$) before and after vortexing, in the presence of *tfoX* induction. Values are the mean of three repeats (±S.D.).

(**E**) Co-culture of fluorescent cells of A1552-Tn*tfoX*, Δ*pilT*, GFP+, producing GFP, and non-fluorescent cells of either *pilA*rep[V52] (A1552-Tn*tfoX*, Δ*pilT*, *pilA*rep[V52]) or *pilA*rep[V52Δtail] (A1552-Tn*tfoX*, Δ*pilT*, *pilA*rep[V52Δtail]), as indicated. Note that ATCC25872 and V52 PilA are identical. Cells were grown in the presence of *tfoX* induction. Merged images show GFP in green and phase-contrast in red. Bar = 25 µm.

Figure 6

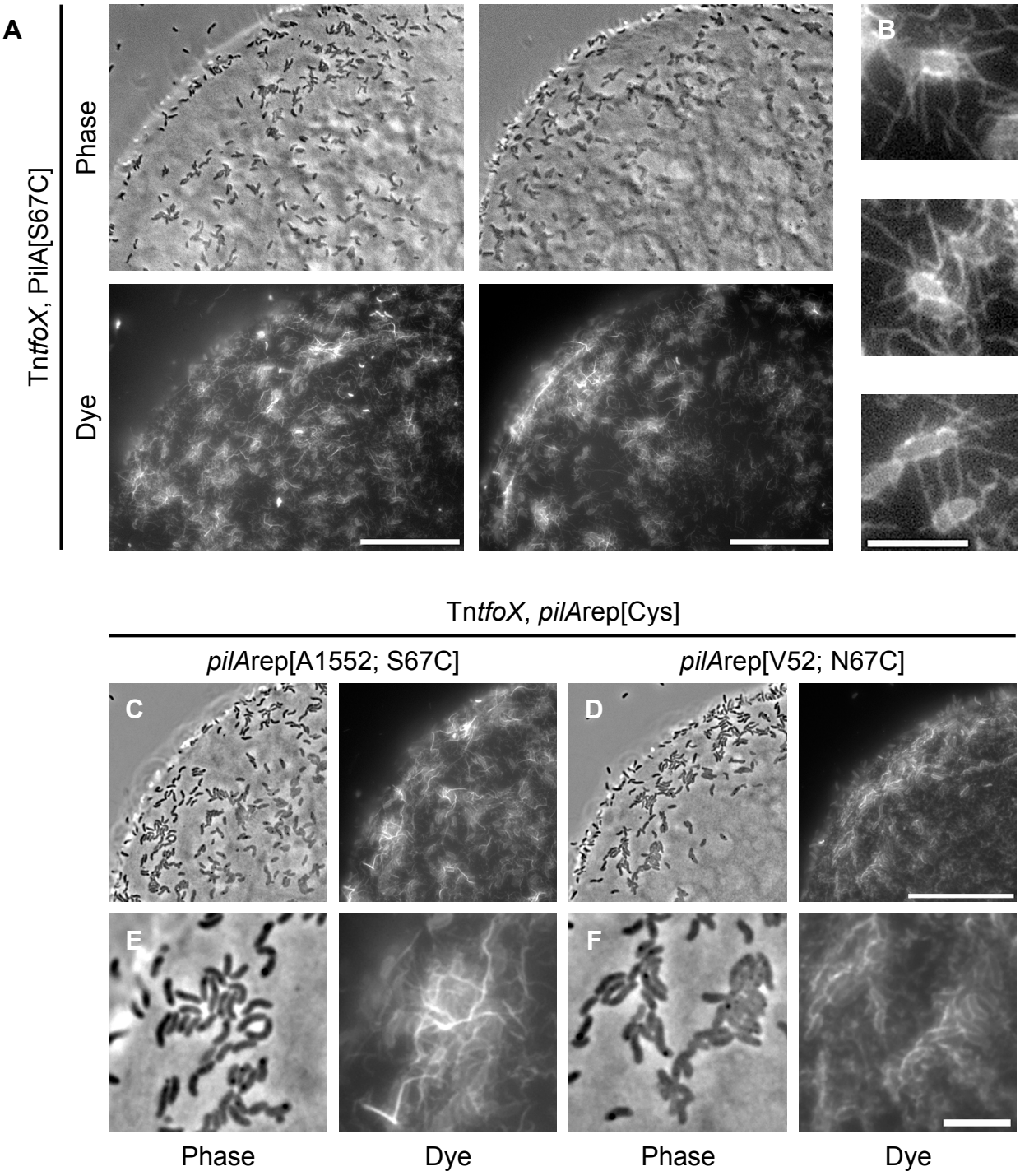

Figure 6. DNA-uptake pili form networks on chitin surfaces.

(**A-B**) Chitin beads were stained with AF-488-Mal after incubation for 48h in defined artificial seawater (DASW) with cells of A1552-Tn*tfoX*, PilA[S67C], as indicated. The figure depicts two separate examples of colonised surfaces, bars = 25 µm. (**B**) Insets show enlarged examples of cells producing multiple pili. Bar = 5 µm.

(**C**-**F**) Chitin beads were stained with AF-488-Mal after incubation for 48h in DASW with cells of either (**C**) A1552-Tn*tfoX*, *pilA*rep[A1552; S67C] or (**D**) A1552-Tn*tfoX*, *pilA*rep[V52; N67C], as indicated. Bar = 25 µm. Panels (**E** and **F**) show enlargements of the surfaces shown in (**C** and **D**). Note the absence of large pili networks in (**F**). Bar = 5 µm.